# HODOSCOPE CALORIMETERS AS BASIC COORDINATE-ENERGY DETECTORS OF PARTICLES IN THE EXPERIMENTS IN THE 10 TeV RANGE

Yu.D. Prokoshkin,
Institute for High-Energy Physics, Serpukhov, USSR.

ABSTRACT

The characteristics of hodoscope hadron and photon calorimeters at superhigh energies have been considered. In the 10 TeV range these detectors are capable of measuring particle energies and coordinates to a high accuracy as well as the masses of unstable particles. This makes their role valuable as basic parts of experimental set-ups at the next-generation accelerators.

## 1. INTRODUCTION

With the growth of energy, the experiments at accelerators are finding wider uses for calorimeters, i.e. detectors able to completely absorb the energy produced by particles and thus to measure their energy. In recent years the hodoscope-type calorimeters, which can measure not only particle energies but also their coordinates, have been developed to detect photons[1-4] and hadrons[5]. The particle coordinates are defined by measuring the energy release of an electromagnetic or hadronic shower in transverse directions. In this case an accuracy of an order of magnitude better than the shower width or calorimeter cell size is attained.

Hodoscope calorimeters[5,6] have been developed as prototypes of detectors designed to be used at superhigh energies. Below we shall consider the possibilities of these set-ups in the 10 TeV range to be realized with the next generation of accelerators (UNK, VBA, etc.).

## 2. HODOSCOPE γ-SPECTROMETER OF THE GAMS TYPE

### 2.1 Hodoscope γ-spectrometers

A characteristic feature of particle interactions at $E \gtrsim 10$ TeV is a large multiplicity of pions and photons in the final state [$\bar{n}_\pi = 1.5 \ln E$ (here and below, E is in GeV), $\bar{n}_\gamma = \ln E$; at E = 20 TeV, $\bar{n}_\gamma \simeq 10$]. Physics done in this energy range requires a detector capable of measuring the coordinates and the energies of tens of photons simultaneously.

Scintillation hodoscope γ-spectrometers[2,3] are sandwich-type detectors, in which iron or lead converters, about 0.5 radiation length ($X_0$) thick, are alternated with hodoscope planes of scintillation counters [648 counters and 2000 scintillators in the NICE spectrometer[2]]. These detectors make it possible to measure the photon coordinates with a precision of better than 2 mm. They have been successfully applied to detect particles decaying into 2-4 photons[3,7]. But with a still larger number of photons the effects of shower overlapping in separate projections become essential, and the accuracy of kinematical reconstruction worsens rapidly.

The GAMS-type hodoscope spectrometer[4-6] is free of these limitations. It is a matrix composed of a large number of total absorption counters [64 × 64 in the case of the NA 12 set-up[6], Fig. 1], whose lateral size is comparable with the electromagnetic shower width (≃ 3 cm). The counter radiators are made of transparent lead glass with an accuracy 0.05 mm.

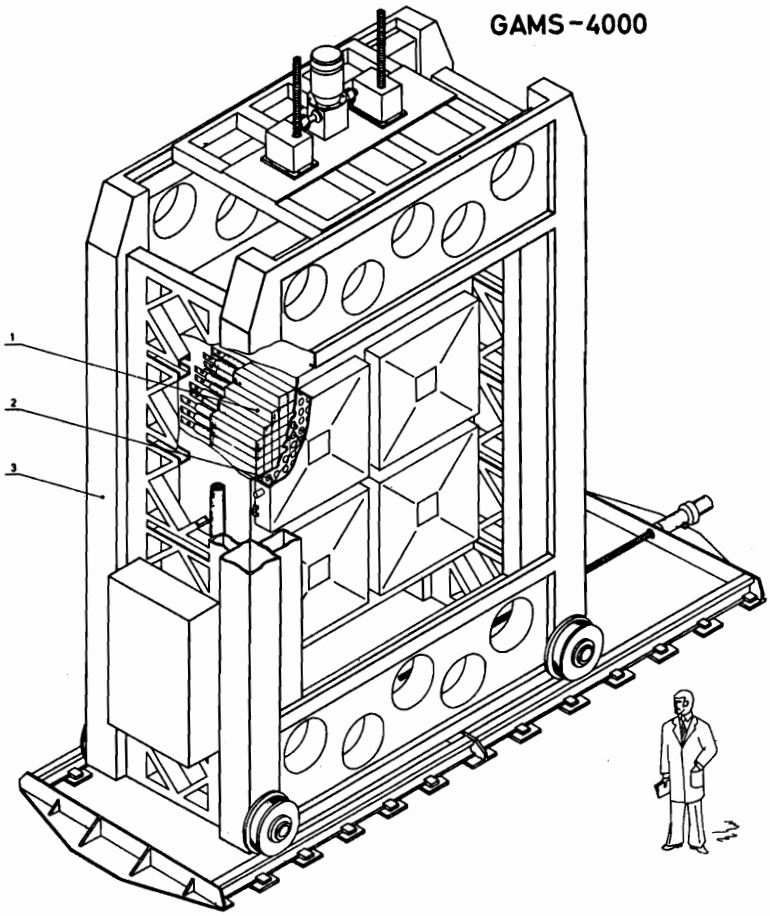


Fig. 1 The schematic representation of the hodoscope γ-spectrometer GAMS 4000 (NA 12 experiment at the CERN SPS): (1) is the cell of 64 × 64 matrix; (2) is the light calibration system; (3) is the platform for moving the spectrometer across the beam.

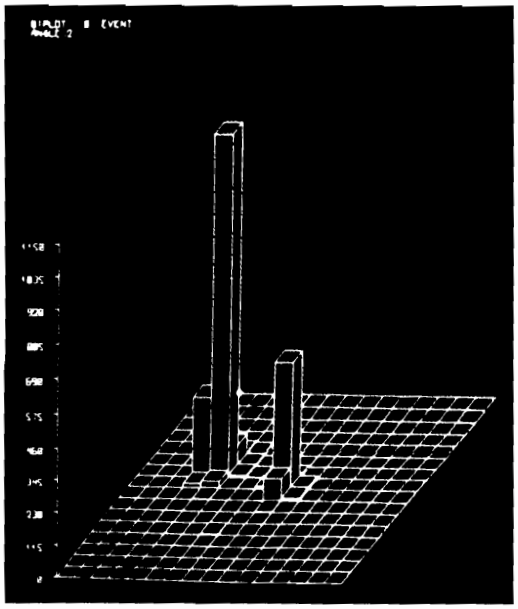

Fig. 2 The display view of the typical 2γ event in the GAMS-200 spectrometer, identified on-line as $\pi^0$ in the reaction $\pi^- p \to \pi^0 n(\pi^0 \to 2\gamma)$ at E = 25 GeV. The vertical axis if for the amplitudes of counter signals.

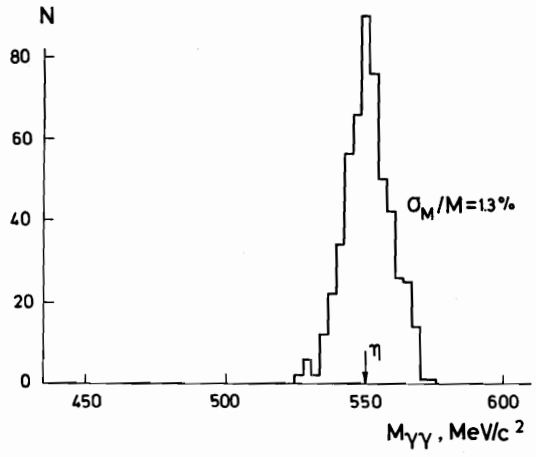


Fig. 3 Mass spectrum of the γ-pairs after a 1C-fit of the events to the reaction $\pi^- p \to M^0 n(M^0 \to 2\gamma)$ (the recoil is assumed to be a neutron). The pointer shows the table value of the η-meson mass.

One early detector of this type, comprising 208 counters, was developed and tested as the model of the GAMS spectrometer for a CERN SPS experiment[6]. With 25 GeV photon energy, the coordinate accuracy obtained was 1.5 mm ($\sigma_y$) and the energy resolution was close to the one achieved in the best lead-glass detectors. The showers produced by neighbouring photons are almost completely separated when the distance between them is $\gtrsim$ 15 cm (Fig. 2). Figure 3 illustrates the possibilities of this device applied as a spectrometer for two-photon states.

The GAMS spectrometer characteristics expected at energies around 10 TeV are discussed below. To extrapolate up to this range, we used the experimental data on the development of showers in lead glass and lead, obtained at energies below 50 GeV, and the shower calculations of showers in lead at higher energies [see survey[8]].

2.2 The choice of the radiator length.
Energy measurement accuracy

Figure 4 presents the characteristic lengths $\ell$ at various photon energies for GAMS counters made of SF-5 lead glass ($X_0$ = 2.36 cm). The distance to the shower maximum $\ell_{max}$ grows logarithmically with energy

$$\ell_{max} = 9 + 3 \ln E \quad \text{(cm)} \tag{1}$$

from 15 cm at E = 20 GeV to 30 cm at E = 20 TeV. The counter length $\ell_\varepsilon$ necessary to absorb the fraction $\varepsilon$ of a shower follows the same dependence. For example,

$$\ell_{0.98} = 28 + 3.8 \ln E \quad \text{(cm)} \ . \tag{2}$$

When $\varepsilon \simeq 1$ the accuracy of energy measurement is weakly dependent on $\varepsilon$:

$$\sigma_E(\varepsilon) = \sigma_E(\varepsilon = 1) \left[1 + 4(1 - \varepsilon) + 50(1 - \varepsilon)^2\right] \tag{3}$$

for an ideally transparent radiator (Fig. 5); for real lead glass, $\sigma_E(\varepsilon)$ and $\sigma_E(\varepsilon = 1)$ differ still less. As seen from Fig. 4, a 60-65 cm cell length is sufficient to absorb the shower completely (98%) at E = 20 TeV. Longer radiators are inexpedient, as in this case the light losses will become appreciable owing to multiple reflections from the radiator facets.

At energies $\gtrsim$ 1 TeV an electromagnetic shower in lead glass develops in its initial state practically without scattering, with its lateral size being << 1 cm. In the case where the range of the measured energies can be limited to $\sim 10^3$ (e.g. detecting photons in the 50 GeV - 10 TeV interval), the GAMS structure can be modified by placing $\sim 4X_0$ thick active converter in front of the basic detector. This could be a matrix composed of larger 9 × 9 cm$^2$ cells (Fig. 6) or a scintillation hodoscope sandwich. The energy released by the shower in the converter should amount to 500 GeV at E = 20 TeV and 4 GeV at E = 50 GeV. The use of an active converter provides the possibility (at a cost of 25% increase of the number of channels in the spectrometer) of strongly increasing the "photon/hadron" rejection and of improving the selectivity of a trigger.

The accuracy of the photon energy measurement in GAMS is determined by the fluctuations of the electromagnetic shower development and Čerenkov light absorption in a radiator [$\sigma_0(E)$], as well as by the photoelectron statistics ($\sigma_{ph} \sim \bar{N}^{1/2}$):

$$\frac{\sigma_E}{E} = \frac{1}{E}\left[\sigma_0^2(E) + \frac{E}{g\xi}\right]^{1/2} . \tag{4}$$

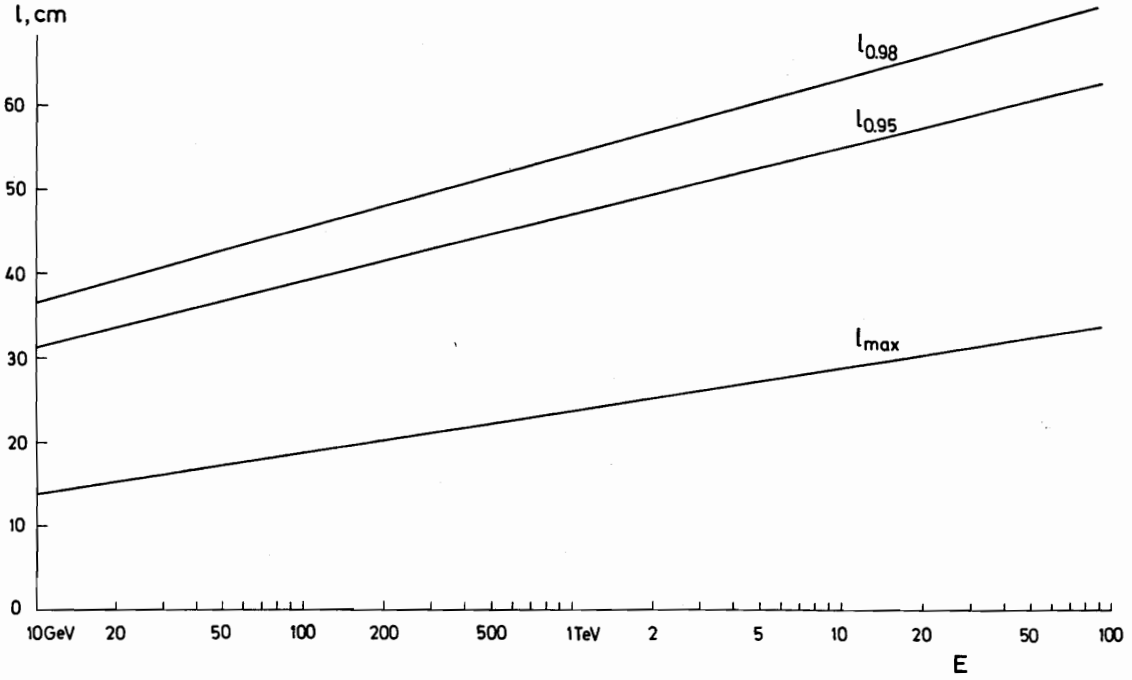


Fig. 4 The characteristic lengths of GAMS, $\ell_\varepsilon$, necessary for the absorption of the fraction $\varepsilon$ of the shower, at various energies. The radiator is SF-5.

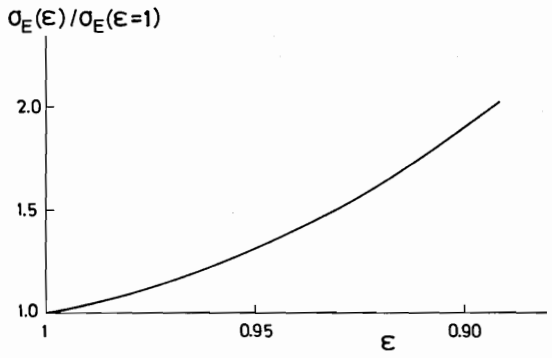


Fig. 5
Energy resolution versus $\varepsilon$ for an ideal radiator

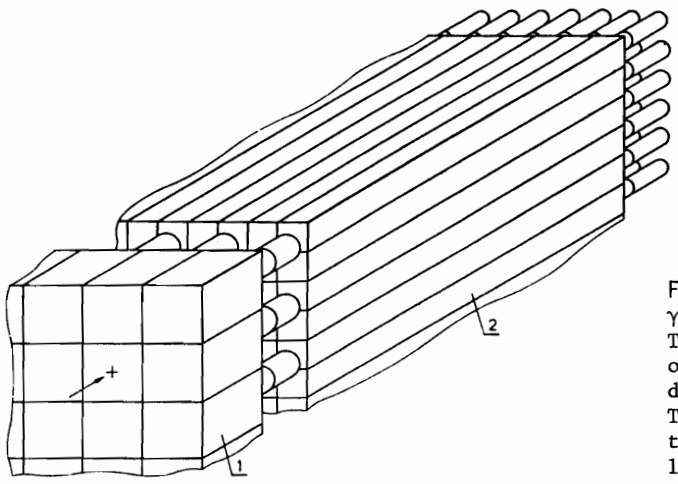


Fig. 6 The schema of the hodoscope $\gamma$-spectrometer with an active converter. The converter cell size is $9 \times 9 \times 10$ cm$^3$ of SF-5 (1). The cell size for the main detector is $4.5 \times 5 \times 55$ cm$^3$ of SF-5 (2). To decrease the distance between the detector and the active converter, the latter can be rotated through 180°.

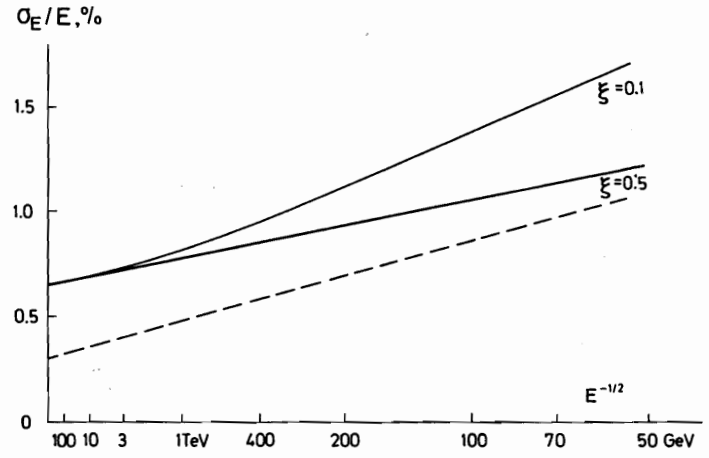


Fig. 7 The accuracy of the photon energy determination in GAMS at $\xi$ = = 0.5 and 0.1 (full lines). The broken line is for the energy resolution when optical filters are used, $\xi = 0.5$.

Here $\xi$ is the ratio of the photomultiplier photocathode area to that of the radiator exit, $\bar{N}_{ph} = g\xi E$, $g \simeq 1000$ photoelectrons per GeV. At $\xi = 0.5$,

$$\sigma_E/E = 0.0064 + 0.042\ E^{-1/2} \qquad (5)$$

(see Ref. 8); $\sigma_0(E)$ can be derived from (4) and (5). With increasing energy, the value of $\sigma_0(E)/E$ decreases more slowly than $E^{-1/2}$ owing to large fluctuations of Čerenkov light absorption. Should a light filter, absorbing the short-wave fraction of the spectrum, be put between the radiator and photomultiplier, the resolution can be appreciably improved (Fig. 7).

When the energy increases, the contribution from the photoelectron statistics to the resolution (4) reduces. Therefore at $E \gg 100$ GeV, a small-size photomultiplier with $\xi \approx 0.1$ can be employed in the GAMS counters without their performance being affected (Fig. 7).

The Čerenkov radiation of a shower is so intense at superhigh energies (at E = 20 TeV, $N_{ph} \simeq 2 \times 10^7$ photoelectrons) that photomultipliers with a small number of dynodes (8-10) can be applied.

Here we shall also note that a relativistic particle emits Čerenkov radiation at a $\bar{N}_{ph} \simeq 10^3$ level in a GAMS counter radiator, which amounts to only $10^{-4}$ of a 10 TeV photon signal. Therefore the background level in GAMS is expected to be exceedingly low at such high energies.

2.3 The choice of a GAMS cell size.
Accuracy of the coordinate measurement

Figure 8 shows the dependence of the coordinate accuracy $\sigma_y$ at E = 25 GeV for the GAMS spectrometer on the cell size d. At d > 5 cm, $\sigma_y$ grows quickly with d:

$$\sigma_y(d) = \sigma_y(d = 0) \cdot e^{d/d_0}\ , \qquad (6)$$

but in a $d \lesssim 3$ cm region it is almost constant. As seen from Fig. 8, a change for a cell smaller than that used in GAMS[6] is not beneficial from the viewpoint of the coordinate accuracy. At the same time, with smaller d the energy resolution losses will grow because of the larger number of light reflections in the radiator.

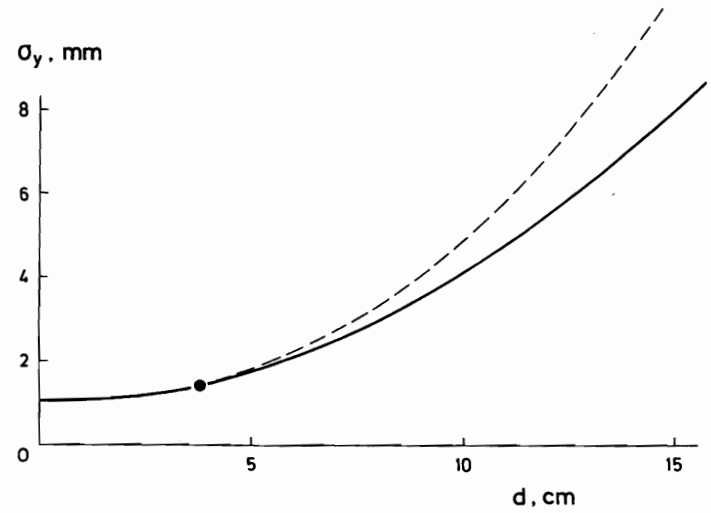


Fig. 8 The dependence of GAMS coordinate accuracy on the size of its cell. The broken line is for the cell centre; the full line is obtained from integrating over the whole cell [at d > 3 cm the latter is described by formula (6) with the parameters $\sigma_y(d = 0) = 0.8$ mm and $d_0 = 6.5$ cm].

When the energy increases, the lateral size of an electromagnetic shower remains almost unchanged. The number of shower particles grows approximately with the energy E. Therefore the coordinate accuracy improves:

$$\sigma_y(E) \simeq \text{const} \cdot E^{-1/2} \tag{7}$$

(this relation holds true for a shower in which the lateral correlations of the number of particles are negligible). Dependence (7) has been checked in the 2-40 GeV range[4].

As seen from formulae (6) and (7), a change for a larger cell d ≃ 45 mm is possible at E ≃ 10 TeV. Even in this case the coordinate resolution will remain $\sigma_y < 0.5$ mm, and it will be determined mainly by the detector manufacturing and calibration accuracy. It is inexpedient to use a cell of larger size since the capability of the spectrometer to distinguish between the adjacent photons will then worsen.

## 2.4 The characteristics of GAMS at E = 20 TeV

When photons coming from the decay of an unstable particle (e.g. $M^0 \to 2\gamma$) hit the GAMS spectrometer, the mass of the particle can be measured:

$$M \simeq (E_{\gamma_1} E_{\gamma_2})^{1/2} \theta_{\gamma\gamma} . \tag{8}$$

Here $\theta_{\gamma\gamma}$ is the opening angle between two photons. Equations (5) and (7) suggest that at E ≳ 10 TeV, the measurement of M should attain a precision $\sigma_M/M \simeq 0.3$-$0.5\%$ (Fig. 9).

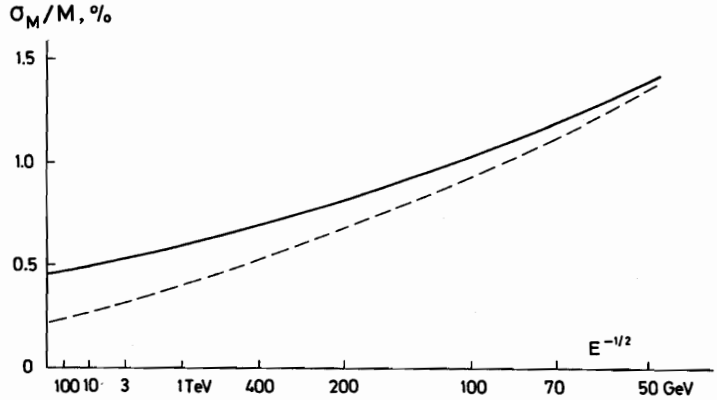


Fig. 9 GAMS resolution on the effective mass (8). As an example, the decay $\chi(3.5) \to 2\gamma$ is taken. The set up geometry is: L = E/50 m. The full line is for the resolution (5); the broken line is for the case when optical filters are used.

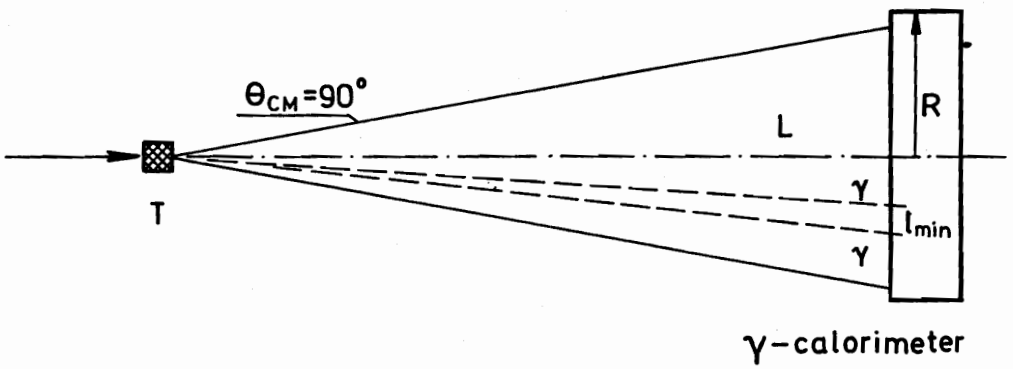


Fig. 10 The geometry of the experiment with GAMS. The pointer shows the beam hitting the target T.

Let us now estimate the necessary dimensions of the spectrometer. Ninety-eight percent of the energy released by a shower in SF-5 type lead glass is concentrated in a cylinder of 10 cm radius. Therefore, a zone of 4 × 4 GAMS cells is required in order to detect one photon. Introducing a factor $K \simeq 50$ to compensate for non-uniform concentration of $\gamma$-showers and the spectrometer "contamination" by hadronic showers (a hadronic shower occupies about 50 cells), and with the maximum multiplicity being $n_\gamma \simeq 20$, we calculate the total number of GAMS cells to be $128 \times 128 \simeq 10^4$ and the aperture to be $\simeq 30$ m$^2$. This is close to the projects[6] being realized at the present moment.

The experimental geometry, with the GAMS spectrometer used at E = 20 TeV (Fig. 10) is determined by the competing requirements. On the one hand, the distance L between the target and the spectrometer has to be long enough for the latter to distinguish efficiently between single photons and $\pi^0$'s yielding $\gamma$ pairs ($\ell_{min} \gtrsim 3$ cm). On the other hand, it has to be short enough for a geometry close to $4\pi$ to be realized.

The former requirement means $L > \ell_{min} \cdot E/\bar{n}_\pi 2m_{\pi^0} = \ell_{min} \cdot E/3 \ln E \cdot m_{\pi^0}$, i.e. at E = 20 TeV, L > 150 m. The latter suggests $R/L \gtrsim (2/E)^{1/2}$ (the r.h.s. of the equation is an angle in the lab. system, corresponding to $\theta_{cms} = 90°$, and R is the detector radius). At E = 20 TeV, $L/R \lesssim 100$, $L \lesssim 300$ m. Thus, taking $L \simeq 280$ m, one can meet both requirements.

Basic parameters of the hodoscope $\gamma$-spectrometer at E = 20 TeV

| | |
|---|---|
| Size of a lead-glass cell | 4.5 × 4.5 × 65 cm$^3$ |
| Glass type | SF-5 |
| Photomultiplier type | Ø 2 cm, 10 dynodes |
| Total number of cells | $1.6 \times 10^4$, 128 × 128 |
| Total weight of the glass | 90 t |
| Useful area of the spectrometer | 30 m$^2$ |
| The target spectrometer distance | 300 m |
| Range of the measured energies | 1 GeV - 20 TeV |
| Stability | 1% |
| $\gamma$ coordinate measurement accuracy | 0.5 mm and better |
| $\gamma$ energy measurement accuracy | 1% |
| Mass resolution of a particle decaying into photons | 1% |

| | |
|---|---|
| Distance between photons, necessary for complete separation of showers | 15 cm |
| Distance between photons, sufficient to distinguish between $\pi^0$ and single $\gamma$ | 3 cm |
| Number of simultaneously detected photons | 30 and more |
| Signal/background (the ratio of $\gamma$ and muon pulse heights) | $2 \times 10^4$ |
| Time resolution | 30 ns |
| Number of accepted events | up to $10^7$/pulse |
| Number of recorded events | up to $10^4$/pulse |
| Calibration time for the spectrometer in the beam | 2-3 days |
| Cost of one channel, electronics (50%) included | SF 800 |
| Total cost | SF $12 \times 10^6$ |
| Manufacturing time | 2-3 years |

## 5. HODOSCOPE HADRON CALORIMETER

When developing a detector designed to measure the hadronic energies and coordinates simultaneously, the same approach as in the case of the scintillation hodoscope $\gamma$-spectrometer is realized. One should only bear in mind that a hadronic shower differs from an electromagnetic one in that its lateral dimensions are larger (by an order of magnitude) and that there are considerable fluctuations and correlations of the number of shower particles. Figure 11 presents a schematic view of a hadron calorimeter[5] developed as a prototype of

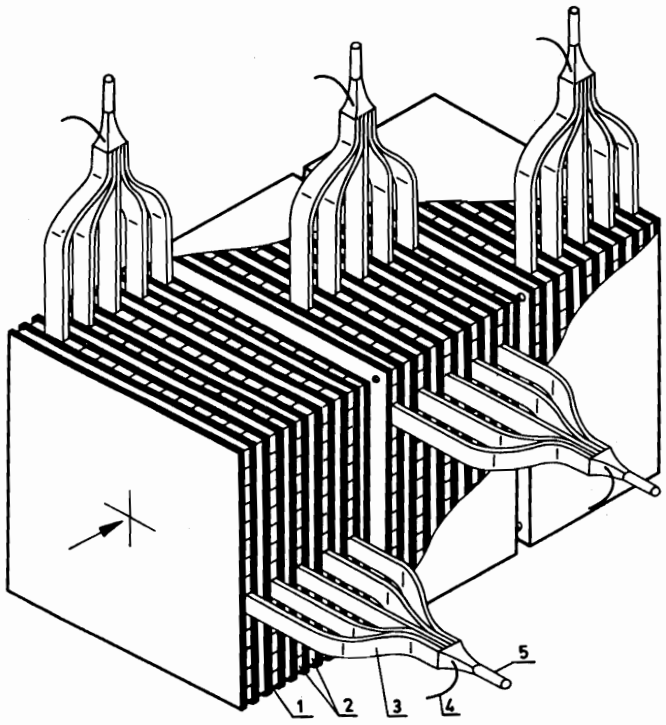


Fig. 11 The schematic view of the hodoscope calorimeter. Five counters (out of 84) are shown in X and Y projections. The calorimeter blocks are: (1) 2.5 cm steel absorber; (2) 1 cm scintillators; (3) the light-guide; (4) the fibre-glass optics of the light calibration system; (5) the photomultiplier.

a detector for superhigh energies and applied in experiments[9] to detect neutral hadrons. Its structure is similar to that of γ-spectrometers[2,3], but the steel converters are made appreciably thicker. The hodoscope element width d was chosen to be 5 cm.

The detector is divided into identical blocks. This enables us to observe the longitudinal development of the showers, and provides a good "hadron/photon" rejection. A transition to higher energies is realized by simply building up the number of blocks (the addition of one block makes a range 30 times wider).

3.1 The calorimeter length.
The measurement accuracy of the hadron energy

The calorimeter length that is necessary for complete absorption of a hadron shower follows a logarithmic dependence similar to (2):

$$\ell_{0.95} = 40 + 9 \ln E \text{ (cm Fe)} . \qquad (9)$$

Formula (9) is verified for energies up to 200 GeV (see Ref. 8). To extrapolate to the 10 TeV range, the calorimeter length increases somewhat more slowly than ln E because of a quicker fractioning of the primary energy due to an increase of multiplicity $n_\pi$ (Fig. 12).

When E = 20 TeV, 120 cm of Fe is needed to absorb a proton-induced shower. Thus to change from tens of GeV to energies $10^3$ times higher, an addition of just two blocks to the three already used in the hodoscope calorimeter[5] is sufficient.

The measurement accuracy of a hadron energy in the calorimeter follows a relationship similar to (5):

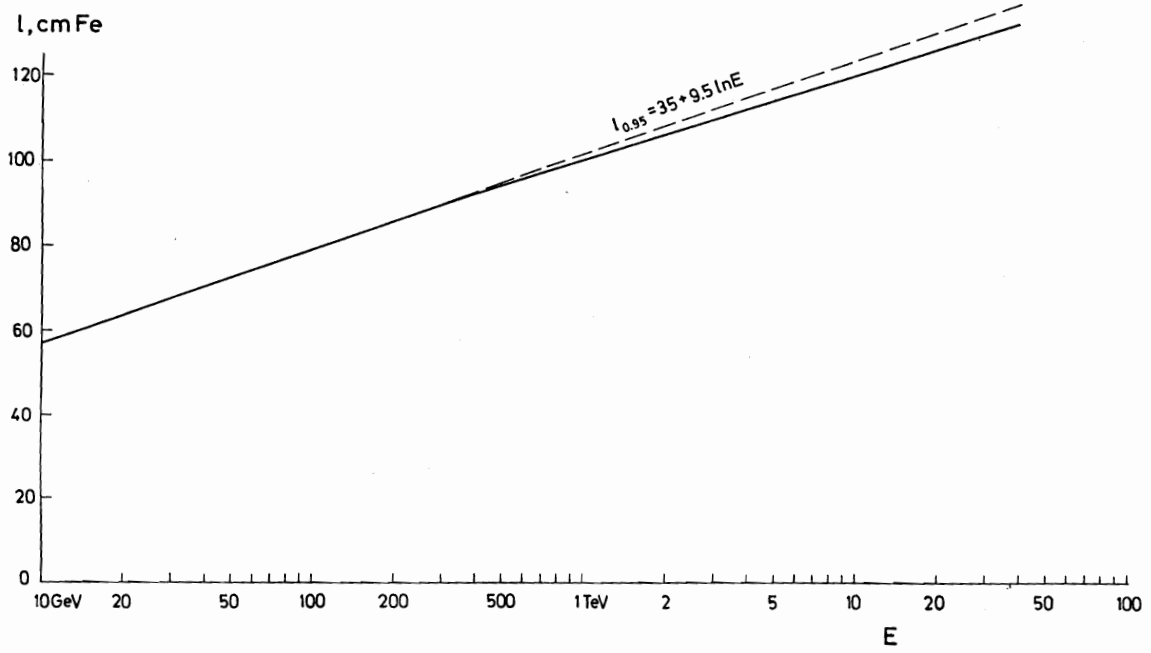


Fig. 12 The length of a hadron calorimeter needed to absorb 95% of the shower, at various photon energies. The broken line shows the dependence (9), the full line gives the growth of the calorimeter length with the account of the increase of multiplicity.

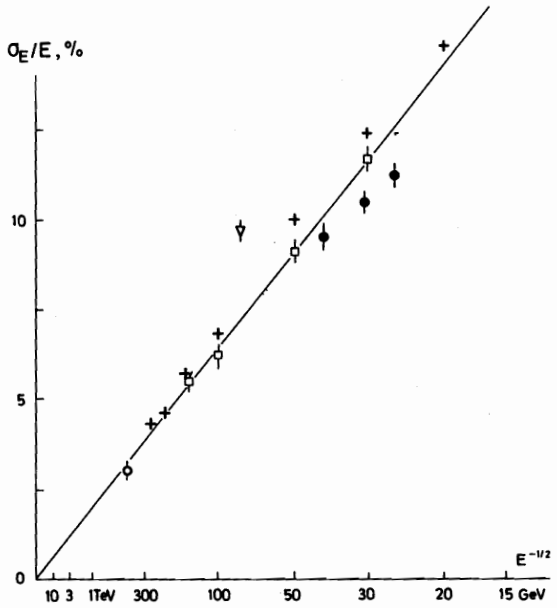


Fig. 13 The accuracy of the hadron energy determination in the calorimeter. □ and + are from Ref. 8; o is CDHS calorimeter, FNAL; • is the hodoscope calorimeter (Ref.5); ▽ is the calorimeter with wavelength shifter. The straight line is the dependence (10). The data are for the converter thickness d = 2.5 cm Fe, using $\sigma_y \sim t^{1/3}$.

$$\sigma_E/E = 0.65\ E^{-1/2} \qquad (10)$$

(Fig. 13). In the ≃ 10 TeV range it reaches ≃ 1%.

The contribution from the photoelectron statistics to the resolution (10) decreases still faster than in the case of γ-detectors. Therefore small-size photomultipliers can be used in calorimeters already in the 10 GeV region.

3.2 The measurement accuracy of hadron coordinates

The hadronic shower profile, as it is seen in a hodoscope calorimeter with a d = 5 cm cell, is shown in Fig. 14. At E = 40 GeV the shower width at the 98% level is 40 cm, which is twice as much as in the case of γ-produced showers in GAMS. The average transverse momentum of particles in a hadronic shower is energy-independent and the longitudinal momentum increases ∼ E/ln E. Apart from this, the fraction of the shower energy carried away by $\pi^0$'s increases. Therefore with increasing energy the width of a hadronic shower decreases slowly, approaching that of an electromagnetic one (15 cm in the steel/scintillator sandwich with the structure of Fig. 11). At E = 20 TeV the hadronic shower will become narrower down to ≃ 25 cm (the 98% level).

The measurement accuracy of hadron coordinates at E = 40 GeV is $\sigma_y$ = 8.5 mm in a calorimeter with a d = 5 cm cell (Fig. 15). It improves at higher energies:

$$\sigma_y = \frac{q_0}{E}\left[\ln^4 E + q_1 E\right]^{1/2} \qquad (11)$$

(Fig. 16), and at E >> 1 TeV the hadron coordinates are likely to be determined to a millimetre accuracy.

An increase in d results in $\sigma_y$ growing in the same way as (6) in the case of a hadronic shower, but with different values of parameters: at E = 40 GeV, $\sigma_0$ = 5.3 mm, $d_0$ = 10 cm (Fig. 17). At superhigh energies it is expedient to change to wider hodoscope elements with d = 10 cm in order to cut down their total number. Even in this case $\sigma_y$ ≃ 1 mm at E ≃ 10 TeV.

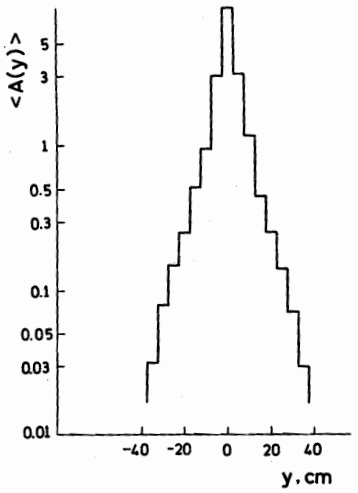


Fig. 14 The average shower profile, measured when the hodoscope calorimeter, was irradiated by 25 GeV antiprotons. The counter signal amplitudes A are normalized on the muon signal.

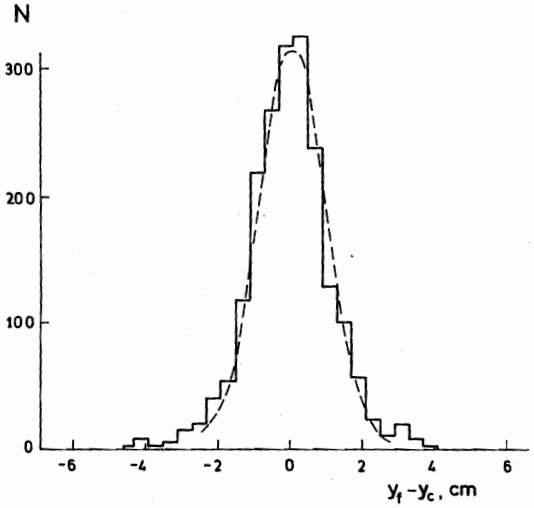


Fig. 15 The distribution for the differences of the measured antiproton coordinates ($y_f$) and the real ones ($y_c$) for d = 5 cm, E = 40 GeV. The broken line is a Gaussian curve.

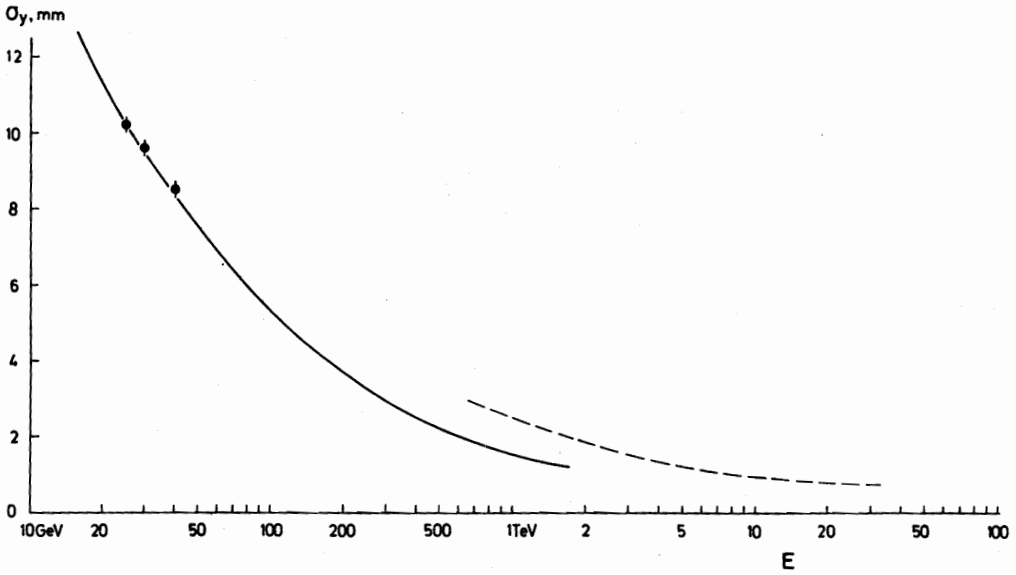


Fig. 16 Hadron coordinate determination accuracy versus the energy. Points are the data (Ref. 5). The full line and the broken line are for formula (11) ($q_0$ = 1.8 cm, $q_1$ = 4 GeV$^{-1}$) at d = 5 and 10 cm, respectively.

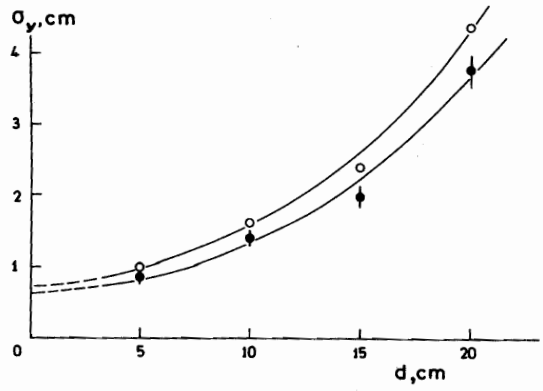


Fig. 17 The dependence of the hadron coordinate determination accuracy on the size of the calorimeter cell d, at E = 25 GeV (o) and E = 40 GeV (•). The curves are the exponential functions (6) with the parameters $d_0$ = 10 cm and $\sigma_y$(d = 0) = 6.0 mm and 5.3 mm, respectively.

### 3.3 The characteristics of a hodoscope hadron calorimeter at E = 20 TeV

In the foregoing, we were considering a hadron calorimeter with a planar hodoscope structure. Using a detector of this type at E ≃ 20 TeV raises difficulties related to shower overlapping in the calorimeter projections when the multiplicity of particles is large. If we confine ourselves to $n_\pi = 10$ and to the factor K, which takes into account a uniformity in the shower concentration, equal to 5, the useful area of the calorimeter will be 100 $m^2$, with the iron weighing about 1000 t. A detector of a still larger size seems today to be hardly realistic.

A cell-structured hadron calorimeter would be able to detect processes of much higher multiplicity. Figure 18 presents a schematic view of a cell of such a detector, made in the form of a steel/scintillator sandwich. The light refraction method is used here to output and sum the light signals from scintillators[10]. Since light loss is large, the energy resolution becomes 1.5 times worse, compared to that of conventional sandwich detectors (Fig. 13). But at E >> 1 TeV the value of a light signal in the scintillator calorimeters becomes so large ($N_{ph} \sim E$) that this compensates for the aforementioned light loss. At E = 20 TeV the energy measurement accuracy in a cell-type hadronic calorimeter will be 1-2%.

To detect one hadronic shower, 3 × 3 cells of the d = 10 cm size are needed. With the maximum multiplicity $n_\pi = 20$ and K = 10, the total number of hadronic calorimeter cells will be $48 \times 48 \times 3 \simeq 7 \times 10^3$ (the detector is divided into three blocks in depth). As the width of the shower is large in the last block, the cell size can be increased to 20 × 20 $cm^2$; this will bring the total cell number down to $5 \times 10^3$. The hadronic calorimeter has the same aperture as the γ-calorimeter (see Section 2.4) and is employed in an experiment with a similar geometry (Fig. 10).

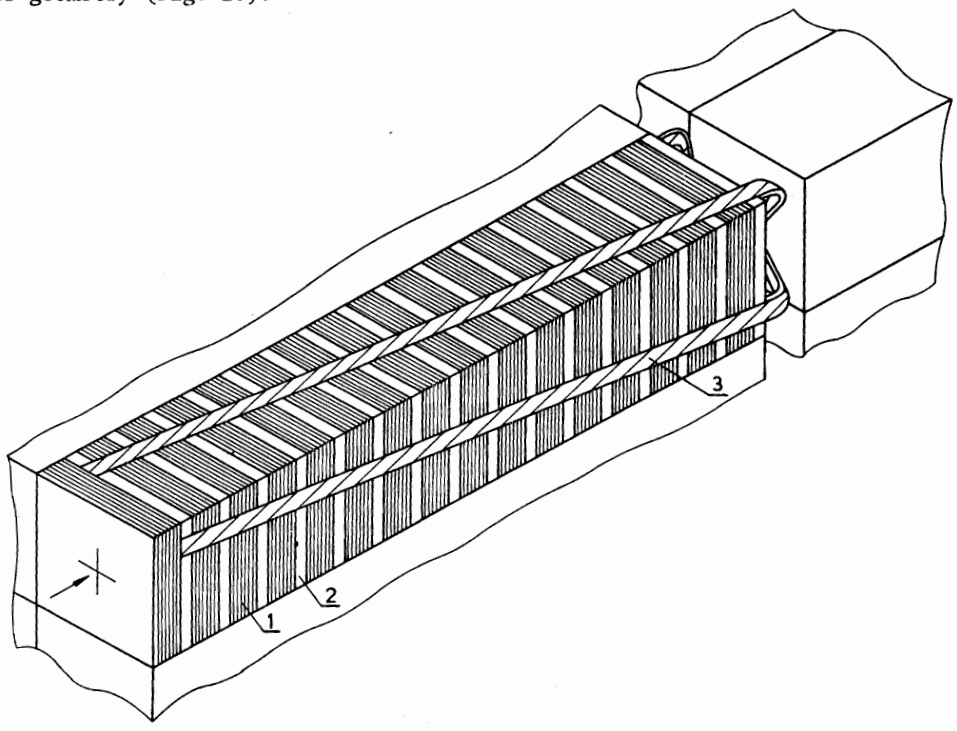


Fig. 18 The schema of the hadron calorimeter cell. The cell structure is shown for the first of three blocks: (1) is 2.5 cm steel converter; (2) is 8 mm scintillator; (3) is the light-guide with the wavelength shifter. The photomultipliers are placed at the end of the cell.

Basic parameters of the hodoscope-type hadron calorimeter at E = 20 TeV

a) Cell-type hodoscope calorimeter

| | |
|---|---|
| Dimensions of a block cell | $10 \times 10$ cm$^2$ $\times$ 40 cm Fe (1st and 2nd blocks), $20 \times 20$ cm$^2$ $\times$ 40 cm Fe (3rd block) |
| Cell structure | (2.5 cm Fe + 0.8 cm scint.) $\times$ 16 |
| Number of blocks (along the beam) | 3 |
| Total thickness of the calorimeter | 120 cm Fe |
| Total number of cells | $5 \times 10^3$, $48 \times 48 \times 2 + 24 \times 24$ |
| Total weight of the iron | 250 t |
| Total weight of the scintillator | 10 t |
| Useful area of the calorimeter | 23 m$^2$ |
| Target-calorimeter distance | 250 m |
| Range of the measured energies | 20 GeV-20 TeV |
| Stability | 1% |
| Hadron energy measurement accuracy | 1-2% |
| Hadron coordinate measurement accuracy | 1 mm |
| Mass resolution of a particle decaying into two hadrons | 2% |
| Distance between two hadrons necessary for complete separation of showers | 30 cm |
| Number of simultaneously detected hadrons | 20 |
| Hadronic and muonic signal ratio | $10^4$ |
| Time resolution | 30 ns |
| Number of accepted events | up to $10^7$/pulse |
| Number of recorded events | up to $10^4$/pulse |
| Cost of one channel, electronics (40%) included | SF 1000 |
| Total cost | SF $10 \times 10^6$ |
| Manufacturing time | 2-3 years |

b) Planar-type hadron calorimeter

| | |
|---|---|
| Dimensions of a block hodoscope element | $10 \times 500$ cm$^2$ $\times$ 40 cm Fe |
| Block structure | (4 cm Fe + 2 cm scint.) $\times$ 10 |
| Number of block hodoscope elements in one projection | 200 |
| Number of blocks (along the beam) | 3 |
| Total calorimeter thickness | 120 cm Fe |
| Total number of hodoscope elements | 1200 |
| Total weight of the iron | 1000 t |
| Total weight of the scintillator | 60 t |
| Useful area of the calorimeter | 100 m$^2$ |
| Target-calorimeter distance | 500 m |
| Number of simultaneously detected hadrons | 10 |
| Number of simultaneously recorded events | up to $10^3$/ pulse |
| Cost of one channel | SF $15 \times 10^3$ |
| Total cost | SF $20 \times 10^6$ |

The remaining characteristics are the same as for the cell-type hadron calorimeter (see above).

## 4. CONCLUSION

With a transition to the E >> 1 TeV energy range (UNK, VBA), hodoscope calorimeters will take a lead and will play the role of basic particle detectors in the majority of experiments. This is due to the following unique features of these detectors:

- the calorimeter length increases only slightly with particle energy;
- the dynamical range of particle energies measured becomes wider, the high linearity being preserved;
- the accuracy of particle coordinate measurement improves and becomes better than 1 mm;
- a hodoscope calorimeter is capable of measuring the coordinates and energies of a large number of particles simultaneously, neutral hadrons included;
- at energies above 1 TeV it becomes a precision spectrometer, enabling reconstruction of the masses of unstable particles from their decay products with a few percent accuracy;
- with hodoscope calorimeters employed, the magnets for determining particle momenta are no longer needed (providing a few percent accuracy is sufficient);
- a geometry close to $4\pi$ can be realized in an experimental set-up employing hodoscope calorimeters;
- cell-type hodoscope calorimeters measure the longitudinal and the transverse constituents of particle momenta directly; therefore the information on the kinematics of the process is transferred in the complete form from the calorimeter to an on-line computer;
- the last point, in particular, makes it possible to a) arrange a selective trigger of the set-up; and b) having handled the data by fast processors, to compress them essentially prior to recording on a magnetic tape.

* * *

## REFERENCES


1) Yu.B. Bushnin et al., Preprint IHEP 72-34, Serpukhov (1972); Nucl. Instrum. Methods 106, 493 (1973).

2) Yu.B. Bushnin et al., Preprint IHEP 74-21, Serpukhov (1974); Nucl. Instrum. Methods 120, 391 (1974).

3) O.I. Dahl et al., Phys. Rev. Lett. 37, 80 (1976).

4) G.A. Akopjanov et al., Preprint IHEP 76-110, Serpukhov (1976); Nucl. Instrum. Methods 140, 441 (1977).

5) F. Binon et al., Preprint IHEP 79-128, Serpukhov (1979).

6) F. Binon et al., Preprint IHEP 78-133, Serpukhov (1978); CERN/SPSC 78-95 Add. (1978).

7) W.D. Apel et al., Phys. Lett. 57B, 398 (1975).

8) S. Iwata, DPNU-3-79, Nagoya University, Japan.

9) G.A. Akopjanov et al., Preprint IHEP 77-3, Serpukhov (1977).

10) V. Eckardt et al., Nucl. Instrum. Methods 155, 389 (1978).